2D Transition Metal Carbide (MXenes) for Energy Conversion and Storage Applications

A
Thesis
Submitted in partial fulfillment of the
requirements for the award of degree of

MASTER OF SCIENCE

by

Gurwinder Kaur

(Registration No. 301704008)

Under the Supervision of

Dr. O.P. Pandey
(Senior Professor & Head)
School of Physics & Material Science,
Thapar Institute of Engineering and Technology (TIET), Patiala - 147004
July 2019

CERTIFICATE

This is to certify that the thesis entitled **'2D transition metal carbide (MXene) for energy conversion and storage applications'** submitted by **Gurwinder Kaur** (Roll no: 301704008) in the fulfilment of the requirement for the award of degree of Masters in Physics in School of Physics & Materials Science, Thapar Institute of Engineering and Technology, Patiala (Punjab), India. It is an exclusive record of candidate's own research under the supervision of Dr. O. P. Pandey. The dissertation in part or full has not been submitted in any other institution for the award of such kind of degree.

Dr. O.P. Pandey

(Supervisor)
Senior Professor & Head
School of Physics and Materials Science
Thapar Institute of Engineering and Technology, Patiala

DECLARATION

I hereby declare that work been presented in the thesis entitled **'2D transition metal carbide (MXene) for energy conversion and storage applications'** by me in partial fulfilment of the requirements for the award of degree of Masters in Physics in School of Physics & Materials Science, Thapar Institute of Engineering and Technology, Patiala is authentic award record on my work carried out under the supervision of Dr. O. P. Pandey, Senior Professor & Head, School of Physics & Materials Science, Thapar Institute of Engineering and Technology, Patiala. The matter in report has not submitted by any other university/Institute for the award of master and science or any other degree.

Gurwinder Kaur

Gurwinder Kaur

301704008

ACKNOWLEDGMENT

First and Foremost, I would like to express my sincere gratitude and respect to my supervisor **Dr. O.P. Pandey** (Senior Professor & Head, School of Physics and Materials Science) for his valuable discussion, strong motivation, devotion and constant encouragement during the work. Secondly, I am thankful to my senior **Mr. Piyush Sharma** for his guidance, great patience, constructive criticism and useful suggestion apart from invaluable guidance to me. I would also like to acknowledge my gratitude towards all the faculty members of School of Physics and Materials Science for their helpful suggestions at different stages of this work.

I heartily thanks to my seniors **Dr. Gurbinder Kaur** and Ph.D. Scholars **Dr. Rameez Ahmad Mir, Ms Ruby Priya, Mrs Shivani Bansal, Mrs Suninderjeet**, **Mr. Puneet Sharma, Ms Raveena Chaudhary**, **Mr. Aayush Gupta**, and **Mr. Sanjay Upadhay** for their moral support, scholarly advice, extensive knowledge and constant co-operation whenever required.

I am especially thankful to my best friends **Mir, Jasvir Kaur** and **Supreet Kaur** for their joyful company, moral support for their encouragement to give my best. I would also thank to my friends **Kajal Rajrana**, **Shweta Chalhotra**, **Ishita Khurana, Navneet Kaur** and **Ali Khan** for their support during the project work.

The meaning of life is incomplete without paying regards to my family whose blessing and continuous encouragement have shown the path to achieve my goals. I am grateful to my Father **Karamjit Singh Bhuller**, Mother **Kiranpal Kaur Bhuller,** loving Grandfather **Harminder Singh Deol** and Grandmother **Jaswant Kaur Deol** for their support in different stages of life. I am also thankful to my loving younger brother **Harmanpreet Singh Bhuller** for his kind support, motivation, care and affection.

Gurwinder Kaur

Gurwinder Kaur

(301704008)

ABSTRACT

MXenes are 2D inorganic compounds which consist of few atoms of thick layers of transition metal carbides, nitrides, or carbonitrides. These materials possess unique combination of properties of transition metal carbides and hydrophilic nature hydroxyl or oxygen terminated surfaces. MXenes are synthesized by the exfoliation of Al layer from the MAX phase. In the present study, Ti_3AlC_2 MAX phase was synthesized by following two different experimental schemes. The major difference between the two schemes was the ball milling duration and handling sample to perform sintering. In scheme I, the sample was ball milled for 15 minutes and pelletized for sintering at different temperatures. Whereas, the pelletized sample was covered with 12 hr ball milled powders for sintering in scheme II. Furthermore, the impact of composition, temperature and dwell time was investigated in both the schemes. The formation of different phases was confirmed through different characterization techniques such as X-ray diffraction (XRD), scanning electron microscopy (SEM), field emission electron microscopy (FE-SEM). The formation of oxides was observed in the sintered samples in scheme I. However, non-oxide phases were observed in the sintered samples in scheme II. The best results were obtained by sintering scheme II sample at 1200 °C with composition Ti/Al/C: 5/5/1.9.

LIST OF FIGURES

CHAPTER 1: INTRODUCTION **PAGE No.**

CHAPTER 3: MATERIALS AND METHODS

CHAPTER 4: RESULT AND DISCUSSION

LIST OF TABLES

CHAPTER 3: MATERIALS AND METHODS **PAGE No.**

CHAPTER 4: RESULT AND DISCUSSION

TABLE OF CONTENTS

PAGE No.

CHAPTER 1: INTRODUCTION

CHAPTER 2: LITERATURE REVIEW

CHAPTER 3: MATERIALS & METHODS

CHAPTER 4: RESULTS & DISCUSSIONS

CHAPTER 5: CONCLUSIONS & FUTURE SCOPE

1.1. Introduction

Nowadays, the technological advancement has led to increase in the demand of energy [1]. The two foremost energy sources are renewable and non-renewable. A huge amount of energy is extracted from non-renewable sources such as coal, petrol and natural gases. The overconsumption of these sources has adverse effect on our environment which has led to global warming and pollution. Moreover, the overconsumption causes the depletion of non-renewable sources [2]. Consecutively, to uphold the growth of the modern society, the scientific community has thought to utilize green energy sources, i.e., wind, water and solar. However, these sources are intermittent in nature [3]. Therefore, it is difficult to convert, and store energy extracted from green energy sources. Thus, the development of an efficient conversion and storage technology is crucial to meet future energy demand.

In this context, the electrochemical devices emerge as suitable candidate for energy storage applications. These devices offer ease of use, high transformation efficiency, and environment friendly [4–6]. In general, the electrochemical devices consist of two metallic or electronic conductors (electrodes) such as anodes and cathodes. These electrodes are commonly made of platinum metal (Pt) because of its good electro-catalytic properties. Though Pt is highly expensive and rare on earth that results into high cost of the electrochemical devices. Hence, there is a great need to develop inexpensive and highly efficient noble metal free electrode material.

Recently, a novel class of 2D layered materials has emerged which includes transition metal carbides, nitrides and carbonitrides. This class of materials is also named as "MXenes" [7]. The MXenes are synthesized through etching layers of '*sp'* element from their corresponding MAX phases. The general formula of MAX phases correspond $M_{n+1}AX_n$ (n = 1, 2, 3) where "M" represents early *d*-block elements (Ti, Sc, V, Cr, Ta, Nb, Zr, Mo, Hf), "A" represents '*sp'* elements of group 13 – 14 and "X" is C or N [8]. MXenes possess three different structures: M_2C, M_3C_2, and M_4C_3. MXenes family consist of nearly 60 members that constitute exclusive properties of both ceramics and metals. MXenes offer high conductivity that makes it a perfect material for battery membranes [9]. Furthermore, there are several MXenes predicted and require processing breakthrough. Hence, it is essential to develop simple synthesis route to obtain novel MXenes.

1.2. What are MXenes?

MXenes were first discovered in 2011 by Naugib and coworkers [10]. These materials possess unique combination of properties of transition metal carbides or nitrides and functional group terminated surfaces [11]. The general formula of MXene is "$M_{n+1}X_nT_x$", here "M" represents transition metals, "X" is carbon and/or nitrogen and "T_x" is the functional group attached with "M" element. The elements considered as "M", "X" and "T_x" in MXenes are shown in Fig. 1.1.

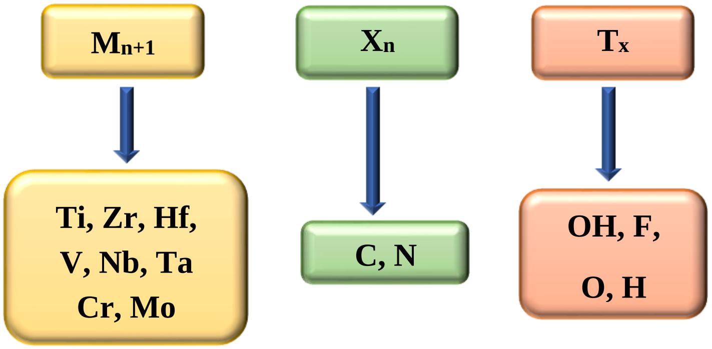

Fig. 1.1: The elements considered as "M", "X" and "T_x" in MXenes.

1.3. Structure of MXenes

MXene's surface is terminated with functional groups, which is obtained through etching of MAX phases. These materials possess nanolaminated hexagonal crystal structures. In MAX phase unit cell, M-M atoms are filled with X-atoms at octahedral site making M_6X octahedra. This structure is similar to the rock salt structure of the MX phases. Also, A-atoms are positioned in the middle of the larger trigonal prism as octahedra alternate with layers. Consequently, larger A-atoms are easily accommodated [5]. Fig. 1.2 shows structure of (M_3AX_2) MAX phase and their corresponding ($M_3X_2T_x$) MXene.

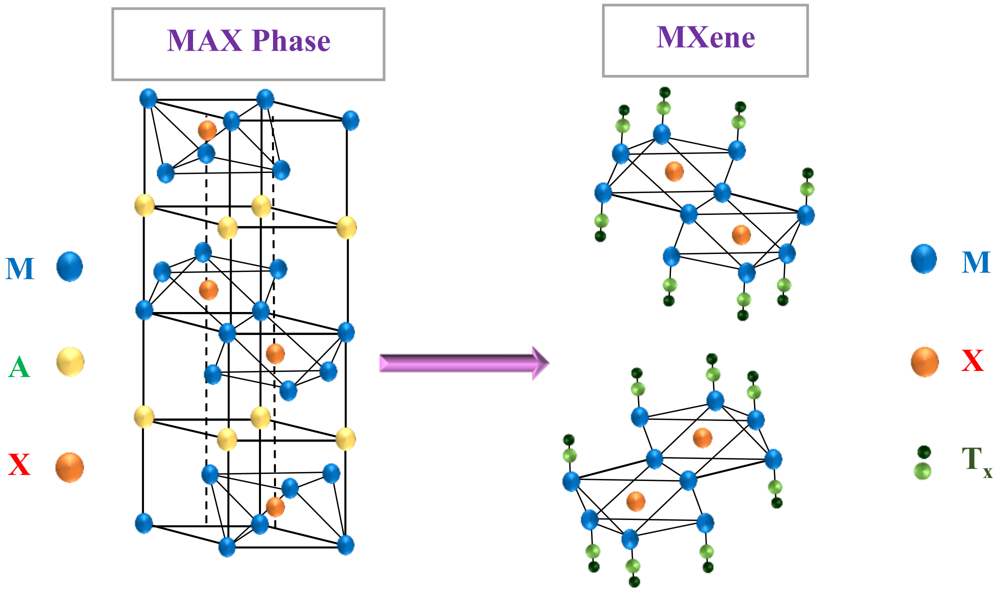

Fig. 1.2: Crystal structure of (M_3AX_2) MAX phase and their corresponding ($M_3X_2T_x$) MXene.

1.4. Synthesis of MXenes

MXenes are synthesized by following three different steps, i.e., (i) synthesis of MAX phase, (ii) exfoliation of “A” layer from MAX phase and (iii) Intercalation/Delamination of MXenes layer [12]. The schematic representation of the synthesis of MXenes is presented in Fig. 1.3. The brief description of the above steps for the synthesis of MXenes is as follows:

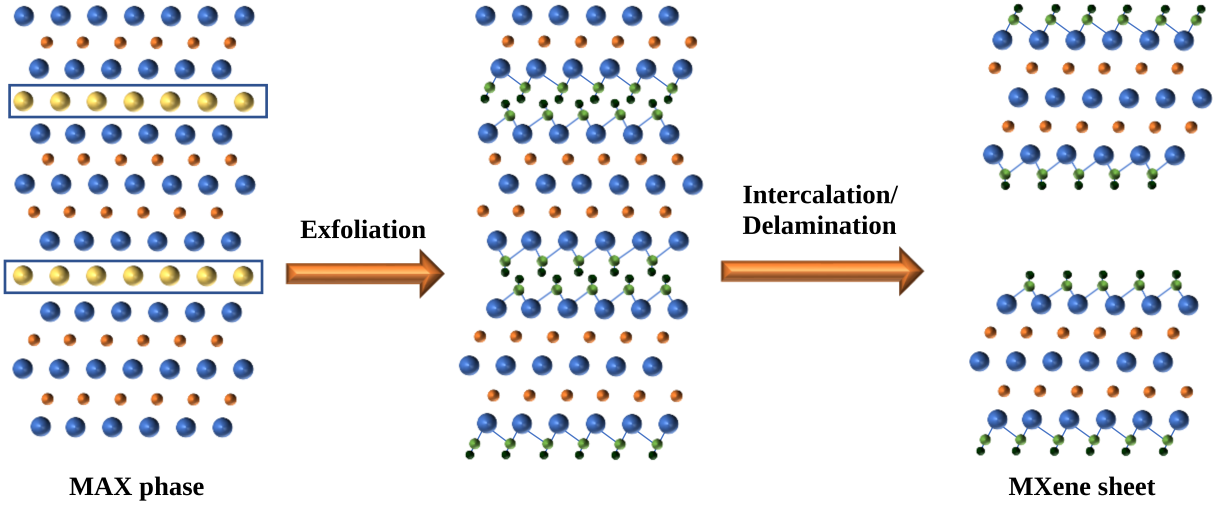

Fig. 1.3: The schematic representation of the synthesis of MXenes.

(i) Synthesis of MAX Phases

Several methods have been reported for the synthesis of the MAX Phases. Numerous researchers follow different sintering techniques such as conventional sintering, spark plasma sintering (SPS), hot isostatic pressing (HIP) and hot pressing (HP) to obtain highly pure nanolaminated MAX phases [13–16]. In the conventional sintering process, no external mechanical pressure is employed on the material during heat treatment. In HIP and HP sintering technique, the external mechanical pressure is induced. Furthermore, electric field is applied to give heat treatment in SPS technique. All the sintering processes are performed in presence of argon environment to avoid the oxidation of the MAX phase.

(ii) Exfoliation of “A” layer from MAX phase

Exfoliation is the process in which ‘A’ element can etched from MAX Phase, to separate the stacked layers into single flakes [17]. The MAX is immersed and stirred or sonicated in acidic solution to obtain MXenes. After acidic treatment, the obtained sample is washed several times in the centrifuge tube, to normalize the pH = 7. In this process, MXenes layers are obtained but there is weak bonding between functional group and transition metal. Hence, intercalation and delamination of exfoliated MAX phase is done to obtain single MXene layer or flake.

(iii) Intercalation and delamination of MXenes

Exfoliated MXenes layers are intercalated to increase the distance between two adjacent layers [18]. In this process, MXenes layers are intercalated with different polar organic molecules and metal ions. After intercalation, single layer 2D MXene is obtained. Furthermore, MXenes layers are treated with organic solvents for the delamination of MXenes.

1.5. Applications of MXenes:

1.5.1. MXenes for Batteries

(i) Li- ion batteries

Pure 2D MXenes and their composites show metallic or thin band gap, semiconducting characteristics and superior electronic properties [3]. Ti_3C_2 MXene is a potential candidate as anode for lithium ion batteries (LIB), due to its small diffusion barrier and operating voltage. Conversion of multilayer MXene into 2D sheet like structure enhances the electrochemical performance [3,19]. The electrochemical activity enhances by optimizing the accurate spacing between the layers of MXenes, which facilitate the transfer of electrolyte ions (adsorption and intercalation) [3].

(ii) Li-S batteries

Lithium sulfur (Li-S) batteries have gained much consideration among the different energy devices due to their high specific capacity (SC) and energy density [3,20]. However, the insulating behavior of discharge products (Li_2S and S) restricts their commercial applications. The highly active 2D surface and exceptional intermetallic character of MXenes makes them probable potential hosts for Li-S batteries. Xie *et al.* determined pure phase MXene (Ti_2C) is an effective cathode material for Li-S batteries [21].

(iii) Non-Li-ion batteries

At the present time, large-scale storage systems utilizing renewable resources and having ability to store more energy for longer duration are required. The practicability of Li for such large-scale electrochemical energy storage devices are hindered, because of relatively lesser abundance of Li in Earth’s crust (only 20 ppm). Consequently, there is an emergent need to develop non-Li-ion batteries (NLIBs) [3,22].

1.5.2. MXenes as supercapacitors

Supercapacitors have attained research interest due to their fast charging/discharging rate, high power density (PD) and superior cyclic stability [3,5]. They are used in hybrid electric vehicles (HEV) and fuel cell vehicles (FCV) start/stop control systems due their high power output [23]. Nowadays, MXene based supercapacitors play a vital role in the energy storage systems. Based on their energy storage mechanism, supercapacitors are mainly classified in two categories, i.e., electrochemical double layer (EDLC,C_{dl}) and pseudo-capacitors. The brief explanation of these supercapacitors is as follows:

(i) Electrochemical double layer capacitors (EDLCs)

EDLCs are based on non-Faradic accumulation of ions within the interface of the electrode and electrolyte [24]. The accommodation of electrolyte ions is directly correlated with the specific surface area (SSA) of the electrode material, therefore it is considered as a critical parameter for enhancing the electrochemical performance of EDLCs. [3,25].

(ii) Pseudo-capacitors

Pseudo-capacitors are based on rapid and reversible Faradic processes. Pseudo-capacitors have attracted considerable attention for energy storage devices due to their higher ability of energy storage with fast charge/discharge rate [26]. The performance of these species depends on the contact between electrode and electrolyte ions. Though, actual mechanism responsible for these interactions has not been explored yet. Zhu *Et al.* [6]investigated the pseudo-capacitor performance of Ti_2CT_x (T = O, F, and OH) nanosheets through first-principles study and revealed the potential use of these species as electrode materials for capacitors.

1.5.3. MXenes as sensors

(i) Electrochemical biosensors:

The utmost characteristics of MXenes such as topography, unexpected surface chemistry, exceptional conducting properties and biocompatibility makes them extremely appropriate for the production of novel bio-sensing devices [4,27]. MXene possess detecting features that can be used to sense immobilization of biological receptors. MXenes biosensors improve the catalytic performances of detecting medium. These sensors holds the bioactivity of enzymes/protein without varying the novel innate conformation [4].

(ii) Solid state gas adsorptive sensors

MXene have determined an inspiring study in gas recognizing applications [28]. The purpose of volatile organic compounds (VOCs) at ultra-trace level (ppb) is important for the detection of pollution, poisonous gases and many viruses while breathing. MXenes constituents are considered as solid-state gas devices due to short electrical sound to detect these gaseous particles with durable signal power and movability [4,29].

(iii) Peizoresistive wearable sensors

Several health regarding issues such as unstable pressure, biological signs and physical spur have been checked with the help of different sensing wearable nano-electronics. MXenes have been used to detect phonations and large activities like walking, hopping, running, coughing, joint twisting [4,30].

(iv) Photoluminescent sensors

These sensors are widely used in photosensitive, biomedical and cellular imaging parts. However, MXenes have shown feasible to develop extremely delicate quantum dots (MQDs) based bioimage sensors. Also, an intracellular photoluminescent ratio metric pH sensor has been established using Ti_3C_2-MQDs for recognition of cell breakdown [4,31].

1.5.4. MXenes for catalysis

MXenes show attractive chemical properties due to their exceptional electroactivity and durability. The catalytic application of MXenes in form of catalyst, co-catalyst and catalyst support have not be widely explored yet [6,32]. Recently, very few catalytic reactions of MXenes have been studied either theoretical or experimental approaches including CO oxidation, dehydrogenation, oxygen reduction reaction (ORR), oxygen evolution reaction (OER) and the hydrogen evolution reaction (HER) [6,33].

References

[1] S. Sun, C. Liao, A.M. Hafez, H. Zhu, S. Wu, Two-dimensional MXenes for energy storage, Chem. Eng. J. (2018). doi:10.1016/j.cej.2017.12.155.

[2] M. Asif, T. Muneer, Energy supply, its demand and security issues for developed and emerging economies, Renew. Sustain. Energy Rev. 11 (2007) 1388–1413. doi:10.1016/j.rser.2005.12.004.

[3] X. Zhang, Z. Zhang, Z. Zhou, MXene-based materials for electrochemical energy storage, J. Energy Chem. 27 (2018) 73–85. doi:10.1016/j.jechem.2017.08.004.

[4] A. Sinha, Dhanjai, H. Zhao, Y. Huang, X. Lu, J. Chen, R. Jain, MXene: An emerging material for sensing and biosensing, TrAC - Trends Anal. Chem. 105 (2018) 424–435. doi:10.1016/j.trac.2018.05.021.

[5] Y. Sun, D. Chen, Z. Liang, Two-dimensional MXenes for energy storage and conversion applications, Mater. Today Energy. 5 (2017) 22–36. doi:10.1016/j.mtener.2017.04.008.

[6] J. Zhu, E. Ha, G. Zhao, Y. Zhou, D. Huang, G. Yue, L. Hu, N. Sun, Y. Wang, L.Y.S. Lee, C. Xu, K.Y. Wong, D. Astruc, P. Zhao, Recent advance in MXenes: A promising 2D material for catalysis, sensor and chemical adsorption, Coord. Chem. Rev. 352 (2017) 306–327. doi:10.1016/j.ccr.2017.09.012.

[7] O. Mashtalir, M. Naguib, V.N. Mochalin, Y. Dall'Agnese, M. Heon, M.W. Barsoum, Y. Gogotsi, Intercalation and delamination of layered carbides and carbonitrides, Nat. Commun. 4 (2013) 1716. doi:10.1038/ncomms2664.

[8] M. Radovic, M.W. Barsoum, MAX phases: Bridging the gap between metals and ceramics, Am. Ceram. Soc. Bull. 92 (2013) 20–27.

[9] H. Tang, Q. Hu, M. Zheng, Y. Chi, X. Qin, H. Pang, Q. Xu, MXene–2D layered electrode materials for energy storage, Prog. Nat. Sci. Mater. Int. (2018). doi:10.1016/j.pnsc.2018.03.003.

[10] M. Naguib, M. Kurtoglu, V. Presser, J. Lu, J. Niu, M. Heon, L. Hultman, Y. Gogotsi, M.W. Barsoum, Two-dimensional nanocrystals produced by exfoliation of Ti_3AlC_2, Adv. Mater. 23 (2011) 4248–4253. doi:10.1002/adma.201102306.

[11] S. Niu, Z. Wang, M. Yu, M. Yu, MXene-Based Electrode with Enhanced Pseudocapacitance and Volumetric Capacity for Power-Type and Ultra-Long Life Lithium Storage, (2018). doi:10.1021/acsnano.8b01459.

[12] Z. Jin, Y. Fang, X. Wang, G. Xu, M. liu, S. Wei, C. Zhou, Y. Zhang, Y. Xu, Ultra-efficient electromagnetic wave absorption with ethanol-thermally treated two-dimensional Nb 2 CT x nanosheets, J. Colloid Interface Sci. 537 (2019) 306–315. doi:10.1016/j.jcis.2018.11.034.

[13] X. Wang, Y. Zhou, Solid–liquid reaction synthesis of layered machinable Ti3AlC2 ceramic, J. Mater. Chem. 12 (2002) 455–460. doi:10.1039/b108685e.

[14] N.C. Ghosh, S.P. Harimkar, Consolidation and synthesis of MAX phases by spark plasma sintering (SPS): A review, Woodhead Publishing Limited, 2012. doi:10.1533/9780857096012.

[15] P. Sharma, O.P. Pandey, Non-isothermal oxidation kinetics of nano-laminated Cr_2AlC MAX phase, J. Alloys Compd. 773 (2019) 872–882. doi:10.1016/j.jallcom.2018.09.326.

[16] Y. Bai, X. He, C. Zhu, G. Chen, Microstructures, electrical, thermal, and mechanical properties of bulk Ti2AlC synthesized by self-propagating high-temperature combustion synthesis with pseudo hot isostatic pressing, J. Am. Ceram. Soc. 95 (2012) 358–364. doi:10.1111/j.1551-2916.2011.04934.x.

[17] M. Naguib, Y. Gogotsi, Synthesis of two-dimensional materials by selective extraction, Acc. Chem. Res. 48 (2015) 128–135. doi:10.1021/ar500346b.

[18] W. Wu, D. Wei, J. Zhu, D. Niu, F. Wang, L. Wang, L. Yang, P. Yang, C. Wang, Enhanced electrochemical performances of organ-like Ti 3 C 2 MXenes/polypyrrole composites as supercapacitors electrode materials, Ceram. Int. 45 (2019) 7328–7337. doi:10.1016/j.ceramint.2019.01.016.

[19] Y. Xie, M. Naguib, V.N. Mochalin, M.W. Barsoum, Y. Gogotsi, X. Yu, K.W. Nam, X.Q. Yang, A.I. Kolesnikov, P.R.C. Kent, Role of surface structure on li-ion energy storage capacity of two-dimensional transition-metal carbides, J. Am. Chem. Soc. 136 (2014) 6385–6394. doi:10.1021/ja501520b.

[20] D. Rao, L. Zhang, Y. Wang, Z. Meng, X. Qian, J. Liu, X. Shen, G. Qiao, R. Lu, Mechanism on the Improved Performance of Lithium Sulfur Batteries with MXene-Based Additives, J. Phys. Chem. C. 121 (2017) 11047–11054. doi:10.1021/acs.jpcc.7b00492.

[21] X. Liu, X. Shao, F. Li, M. Zhao, Anchoring effects of S-terminated Ti2C MXene for lithium-sulfur batteries: A first-principles study, Appl. Surf. Sci. 455 (2018) 522–526. doi:10.1016/j.apsusc.2018.05.200.

[22] Y. Xie, Y. Dall'Agnese, M. Naguib, Y. Gogotsi, M.W. Barsoum, H.L. Zhuang, P.R.C. Kent, Prediction and characterization of mxene nanosheet anodes for non-lithium-ion batteries, ACS Nano. 8 (2014) 9606–9615. doi:10.1021/nn503921j.

[23] C. Du, J. Yeh, N. Pan, High power density supercapacitors using locally aligned carbon nanotube electrodes, 350 (2005). doi:10.1088/0957-4484/16/4/003.

[24] R.A. Mir, O.P. Pandey, Influence of graphitic/amorphous coated carbon on HER activity of low temperature synthesized B-Mo2C@C nanocomposites, Chem. Eng. J. 348 (2018) 1037–1048. doi:10.1016/j.cej.2018.05.041.

[25] G. Wang, L. Zhang, J. Zhang, A review of electrode materials for electrochemical supercapacitors, Chem. Soc. Rev. 41 (2012) 797–828. doi:10.1039/c1cs15060j.

[26] M. Ghidiu, M.R. Lukatskaya, M.Q. Zhao, Y. Gogotsi, M.W. Barsoum, Conductive two-dimensional titanium carbide "clay" with high volumetric capacitance, Nature. 516 (2015) 78–81. doi:10.1038/nature13970.

[27] M. Soleymaniha, M.A. Shahbazi, A.R. Rafieerad, A. Maleki, A. Amiri, Promoting Role of MXene Nanosheets in Biomedical Sciences: Therapeutic and Biosensing Innovations, Adv. Healthc. Mater. 8 (2019). doi:10.1002/adhm.201801137.

[28] B. Xiao, Y.C. Li, X.F. Yu, J.B. Cheng, MXenes: Reusable materials for NH 3 sensor or capturer by controlling the charge injection, Sensors Actuators, B Chem. (2016). doi:10.1016/j.snb.2016.05.062.

[29] J. Guo, Q. Peng, H. Fu, G. Zou, Q. Zhang, Heavy-Metal Adsorption Behavior of Two-Dimensional Alkalization-Intercalated MXene by First-Principles Calculations, J. Phys. Chem. C. 119 (2015) 20923–20930. doi:10.1021/acs.jpcc.5b05426.

[30] R. Paradiso, G. Loriga, N. Taccini, A Wearable Health Care System Based on Knitted

Integrated Sensors, 9 (2005) 337–344.

[31] X. He, X. Hu, T.D. James, Chem Soc Rev Multiplexed photoluminescent sensors : towards improved disease diagnostics, (2017). doi:10.1039/c6cs00778c.

[32] C.E. Ren, M.Q. Zhao, T. Makaryan, J. Halim, M. Boota, S. Kota, B. Anasori, M.W. Barsoum, Y. Gogotsi, Porous Two-Dimensional Transition Metal Carbide (MXene) Flakes for High-Performance Li-Ion Storage, ChemElectroChem. 3 (2016) 689–693. doi:10.1002/celc.201600059.

[33] M. Pandey, K.S. Thygesen, Two-Dimensional MXenes as Catalysts for Electrochemical Two-dimensional MXenes as Catalysts for Electrochemical Hydrogen Evolution : A Computational Screening Study, (2017).

2.1. Literature review

$Ti_3C_2T_x$ MXene has gained substantial attention from the scientific community due to its wide range of applications, such as electrode material, hydrogen storage, lead adsorption medium, electrocatalyst and photocatalyst. Synthesis of Ti_3C_2Tx is complex and involves preparation of the Ti_3AlC_2 MAX phase, followed by MAX phase etching using a strong oxidizing agent. Many researchers investigated the synthesis of the MAX phase and MXenes. The brief explanation of the work done related to synthesis of MXenes and their applications are as follows:

In 2011, Naguib *et al.* [1] firstly prepared Ti_3C_2Tx MXene through etching of Ti_3AlC_2 MAX phase in hydrofluoric acid (HF) solution. They synthesized Ti_3AlC_2 through hot pressing of Ti_2AlC and TiC milled powder at 1350°C for 2 h in the presence of argon. The study demonstrated potential synthesis route to produce MXenes through etching of MAX phases. Further, they also reported various MXenes (Ti_2C, Ta_4C_3, Nb_2C, V_2C, Ti_3CN, $(V_{0.5}Cr_{0.5})_3C_2$, and $(Ti_{0.5}Nb_{0.5})_2C$) through etching of Al-based MAX phases (Ti_2AlC, Nb_2AlC, V_2AlC, Ta_4AlC_3, Ti_3AlCN, $(V_{0.5}Cr_{0.5})_3AlC_2$, and $(Ti_{0.5}Nb_{0.5})_2AlC$) [2-5]. They examined the electrochemical properties of Nb_2CTx and V_2CTx and measured reversible capacitance at lower lithiation. It was found that V_2CTx MXene possess best reversible capacitance of 260 $mAhg^{-1}$ at 1 C. This was the first report that provides strong evidence of fast Li diffusion in MXenes.

The tribological properties of Ti_3C_2 MXene were also investigated [6]. It was reported that only 1.0 wt% Ti_3C_2 MXene was enough to increase the friction-reducing and antifriction properties of paraffin base oil. In the study, Ti_3AlC_2 MAX phase was prepared through pressureless sintering and Ti_3C_2 MXene was obtained by HF etching of T_3AlC_2 MAX phase. The study provides strong evidence for the development of high-performance 2D lubricating materials based on MXenes. Further, the thermal stability of Ti_3C_2 MXene was studied in oxygen and argon atmosphere [7]. They observed that Ti_3C_2 shows high thermal stability in an inert environment. In oxidative environment, Ti_3C_2 MXene oxidized to anatase nanocrystal at ~ 200 °C and converts into rutile phase at 1000 °C.

The two-dimensional Ti_3C_2 was also studied as anode material for Li-ion batteries [8]. It was observed that the F-group terminated Ti_3C_2 MXene intercalated with dimethyl sulfoxide emerged as promising anode material for Li-ion batteries. The results showed higher capacitance of Ti_3C_2 MXene. The study suggested that F terminated MXenes are highly suitable for anode material.

Ghidiu and his co-workers [9] produced Ti_3C_2 MXene by etching Ti_3AlC_2 in the solution of lithium fluoride and hydrochloric acid. The volume of hydrated MXene swells and exhibit the capability to transform into various shapes like clay. This material can be dried to form highly conductive films. The value of volumetric capacitance was found to be increased up to 900 Fcm^{-3} along with high cyclability. This study indicated that MXenes can be synthesized without using hazardous hydrofluoric acid. Later, they also synthesized new 2D transition metal carbide Nb_4C_3 by etching Nb_4AlC_3 with HF solution [10]. They measured resistivity of a cold-pressed disc of Nb_4C_3 MXene (0.0046 Ω m) and concluded that MXenes are one the most conductive materials.

Wang *et al.* [11] investigated the pseudo-capacitance of Ti_2C MXene nanosheets. The nanosheets showed a higher specific capacity as compared to the double-layered capacitor. It was also observed that the Ti_2C nanosheets had excellent potential attributed to the ion intercalation of electrodes. They employed Ti_2C material as a negative electrode and Na-ion having $Na_2Fe_2(SO_4)_3$ as a positive electrode. The results revealed that the negative electrode of MXene can be operated at high voltage 2.4 V.

In 2016, Feng *et al.* [12] synthesized Ti_3C_2 MXenes by exfoliation of Ti_3AlC_2 MAX phase by using the bi-fluoride solutions ($NaHF_2$, KHF_2 and NH_4HF_2). The study presented safer way to etch MAX phases to obtain MXenes.

Tang *et al.* [13] synthesized 2D nanosheets of Ti_3C_2 MXene. They studied the impact of etching times (2, 6, 24, 72, 120, 168, and 216 h) on the morphology, structure, surface termination, and electrochemical properties of Ti_3C_2 MXene. It was observed that the electrochemical properties of Ti_3C_2 improves with increase in etching time. The higher capacitive performance with the specific capacitance of 118 $F\ g^{-1}$ at the scan rate of 5 $mV\ s^{-1}$was observed in Ti_3C_2 MXene obtained after etching of Ti_3AlC_2 for 216 hours.

Han and co-workers [14] prepared Ti_3C_2 MXene with chemically active surfaces via etching of Ti_3AlC_2. They tuned the surface terminated group through rapid annealing. It was observed that the rapid annealing of MXenes results in change in microwave absorbing and shielding behaviors. After the rapid annealing, the characteristic morphology of MXene remains and a localized sandwich structure was observed. This results into enhancement in the electro-magnetic absorbing capability of Ti_3C_2 MXene. They demonstrated that MXenes are the promising candidate for the development of high-performance electro-magnetic absorbing and shielding materials. Liu and Li [15] synthesized Ti_3C_2 and Ti_2C MXenes by etching the Al from Ti_3AlC_2

and Ti_2AlC MAX phases. They measured the methane adsorption capacity of Ti_3C_2 and Ti_2C MXenes. The results showed that T_2C MXene (11.2 cm^3/gm) adsorb more methane as compared to T_3C_2 (8.5 cm^3/gm). The study suggested that MXenes are potential material to adsorb methane or other harmful gases.

Further, V_2C MXene was prepared through etching of V_2AlC [16]. The prepared V_2C MXene showed high-performance as anode material in Li-ion batteries. At charge rate 500 mAg^{-1}, the capacity of V_2C MXene increased with number of cycles. They reported that the electrochemical properties significantly depend on the phase purity of the MXenes.

Nanoribbons of Ti_3C_2 MXene were prepared through a shaker, in which Ti_3C_2 immersed in KOH solution was kept for 72 h in an argon atmosphere [17]. This result into more interspacing between the layers of Ti_3C_2 and a 3D interconnected Ti_3C_2 MXene nanoribbons were obtained. The nanoribbons as anode material showed extraordinary Na/K storage capacity. High reversible capacities were observed in the case of sodium ion batteries (168 and 136 $mAh\ g^{-1}$ at 20 $mAh\ g^{-1}$) and potassium ion batteries (84 and 78 $mAh\ g^{-1}$ at 200 $mAh\ g^{-1}$). Also, the nanoribbons were highly stable up to 500 cycles at current density of 200 $mAh\ g^{-1}$. The nanoribbons of MXenes are promising anode material for both sodium ion batteries and potassium ion batteries.

Zhu and his co-workers [18] utilized Ti_3C_2 MXenes for the sensing of the heavy metals with high efficiency. They compared the sensing performance of Ti_3C_2 MXene terminated with different functional groups, i.e., alkaline and fluoride groups. It was observed that the alkaline group terminated MXenes are more efficient for sensing heavy metals. The Ti_3C_2 MXene was also used as gas sensing materials at room temperature [19]. Various volatile organic compound gasses were measured through the Ti_3C_2. A p-type sensing behavior was observed in the Ti_3C_2 MXene. The versatile gas sensing behavior of Ti_3C_2 makes it suitable for the development of innovative sensors for wearable electronic devices. Kim *et al.* [20] synthesized Mo based MXenes, i.e., Mo_2CT_x, $Mo_2TiC_2T_x$, and $Mo_2Ti_2C_3T_x$. They investigated the electrical and thermoelectric properties of the prepared MXenes. $Mo_2TiC_2T_x$ showed better results as compared to other two MXenes. A higher value of thermoelectric power ($3.09 \times 10^{-4} Wm^{-1}\ K^{-2}$) and electrical conductivity (1380 $S\ cm^{-1}$) at 803 K was observed in $Mo_2TiC_2T_x$ MXene.

Further, it was proposed that hydrothermal synthesis method can be used for the etching of MAX phases (Nb_2AlC and Ti_3AlC_2) to obtain Nb_2C and Ti_3C_2 MXenes [21]. It was reported that the adsorption properties improved in the prepared MXenes. The study suggested that hydrothermal etching is effective for the synthesis of MXenes with improved properties.

Ali *et al*. [22] reported the effect of synthesis method on the 2D heterostructures of MXene/ Fe_2O_3 nanocomposite. The results of the formation of $Ti_3C_2T_x$/ Fe_2O_3 composite with ball milling method was better than the hydrothermal and sonication method. The composition of 2D heterostructure nanocomposite was optimized to develop highly efficient anode materials. The result revealed that $Ti_3C_2T_x$ – 50 wt% Fe_2O_3 composites offer high reversible specific capacity and performance rate. Furthermore, hydrogen storage capacity of lithium borohydride ($LiBH_4$) was improved with the addition of Ti_3C_2 MXene [23]. This results into increase in the rate of dehydrogenation and decreases the temperature of dehydrogenation. The composition (60wt% $LiBH_4$ milled with 40 wt% Ti_3C_2) demonstrated superior hydrogen desorption property.

Jin *et al.* [24] treated a Nb_2CT_x MXene with two different solutions (ethanol and deionized water) via solvothermal process to improve its electromagnetic wave adsorption property. MXene treated with ethanol showed higher electromagnetic wave absorbing property. Wu and co-worker [25] prepared composite of Ti_3C_2 MXenes and Polypyrrole (PPy) through in-situ polymerization. The PPy increased interlayer spacing of Ti_3C_2 due to which conductivity and charge transfer improved. The results demonstrated that, the highest specific capacitance and good cycling stability of the organ-like nanocomposites of the Ti_3C_2/PPy than the Ti_3C_2 MXene.

Guo *et al.* [26] reported the MXenes as a promising catalyst for the photocatalytic hydrogen evolution reaction (HER). Ti_2C, Ti_3C_2, Nb_2C and V_2C MXenes have shown a good conductive property. The results showed a high charge transfer rate in HER due to the most stable state of the MXenes (Ti_2C, Ti_3C_2, and V_2C) terminated with oxygen and hydroxyl.

Liu *et al.* [27] synthesized a nitrogen doped Nb_2CT_x MXenes as anode materials with improved reversible capacity for Li-ion batteries. They synthesized a nitrogen doped Nb_2CT_x MXene through hydrothermal method. The reversible capacity of nitrogen doped and undoped MXene is 360 mAh/g at 0.2 C and 190 mAh/g at 0.2 C. Further, Cheng and co-workers [28] modified the structure Ti_3C_2 MXene through calcination in different conditions. It was observed that the change in structure of MXenes significantly affects the Li-ion storage capacity.

References

[1] S. Sun, C. Liao, A.M. Hafez, H. Zhu, S. Wu, Two-dimensional MXenes for energy storage, Chem. Eng. J. (2018). doi:10.1016/j.cej.2017.12.155.

[2] M. Asif, T. Muneer, Energy supply, its demand and security issues for developed and emerging economies, Renew. Sustain. Energy Rev. 11 (2007) 1388–1413. doi:10.1016/j.rser.2005.12.004.

[3] X. Zhang, Z. Zhang, Z. Zhou, MXene-based materials for electrochemical energy storage, J. Energy Chem. 27 (2018) 73–85. doi:10.1016/j.jechem.2017.08.004.

[4] A. Sinha, Dhanjai, H. Zhao, Y. Huang, X. Lu, J. Chen, R. Jain, MXene: An emerging material for sensing and biosensing, TrAC - Trends Anal. Chem. 105 (2018) 424–435. doi:10.1016/j.trac.2018.05.021.

[5] Y. Sun, D. Chen, Z. Liang, Two-dimensional MXenes for energy storage and conversion applications, Mater. Today Energy. 5 (2017) 22–36. doi:10.1016/j.mtener.2017.04.008.

[6] J. Zhu, E. Ha, G. Zhao, Y. Zhou, D. Huang, G. Yue, L. Hu, N. Sun, Y. Wang, L.Y.S. Lee, C. Xu, K.Y. Wong, D. Astruc, P. Zhao, Recent advance in MXenes: A promising 2D material for catalysis, sensor and chemical adsorption, Coord. Chem. Rev. 352 (2017) 306–327. doi:10.1016/j.ccr.2017.09.012.

[7] O. Mashtalir, M. Naguib, V.N. Mochalin, Y. Dall'Agnese, M. Heon, M.W. Barsoum, Y. Gogotsi, Intercalation and delamination of layered carbides and carbonitrides, Nat. Commun. 4 (2013) 1716. doi:10.1038/ncomms2664.

[8] M. Radovic, M.W. Barsoum, MAX phases: Bridging the gap between metals and ceramics, Am. Ceram. Soc. Bull. 92 (2013) 20–27.

[9] H. Tang, Q. Hu, M. Zheng, Y. Chi, X. Qin, H. Pang, Q. Xu, MXene–2D layered electrode materials for energy storage, Prog. Nat. Sci. Mater. Int. (2018). doi:10.1016/j.pnsc.2018.03.003.

[10] M. Naguib, M. Kurtoglu, V. Presser, J. Lu, J. Niu, M. Heon, L. Hultman, Y. Gogotsi, M.W. Barsoum, Two-dimensional nanocrystals produced by exfoliation of Ti_3AlC_2, Adv. Mater. 23 (2011) 4248–4253. doi:10.1002/adma.201102306.

[11] S. Niu, Z. Wang, M. Yu, M. Yu, MXene-Based Electrode with Enhanced Pseudocapacitance and Volumetric Capacity for Power-Type and Ultra-Long Life Lithium Storage, (2018). doi:10.1021/acsnano.8b01459.

[12] Z. Jin, Y. Fang, X. Wang, G. Xu, M. liu, S. Wei, C. Zhou, Y. Zhang, Y. Xu, Ultra-efficient electromagnetic wave absorption with ethanol-thermally treated two-dimensional Nb 2 CT x nanosheets, J. Colloid Interface Sci. 537 (2019) 306–315. doi:10.1016/j.jcis.2018.11.034.

[13] X. Wang, Y. Zhou, Solid–liquid reaction synthesis of layered machinable Ti3AlC2 ceramic, J. Mater. Chem. 12 (2002) 455–460. doi:10.1039/b108685e.

[14] N.C. Ghosh, S.P. Harimkar, Consolidation and synthesis of MAX phases by spark plasma sintering (SPS): A review, Woodhead Publishing Limited, 2012. doi:10.1533/9780857096012.

[15] P. Sharma, O.P. Pandey, Non-isothermal oxidation kinetics of nano-laminated Cr_2AlC MAX phase, J. Alloys Compd. 773 (2019) 872–882. doi:10.1016/j.jallcom.2018.09.326.

[16] Y. Bai, X. He, C. Zhu, G. Chen, Microstructures, electrical, thermal, and mechanical

properties of bulk Ti2AlC synthesized by self-propagating high-temperature combustion synthesis with pseudo hot isostatic pressing, J. Am. Ceram. Soc. 95 (2012) 358–364. doi:10.1111/j.1551-2916.2011.04934.x.

[17] M. Naguib, Y. Gogotsi, Synthesis of two-dimensional materials by selective extraction, Acc. Chem. Res. 48 (2015) 128–135. doi:10.1021/ar500346b.

[18] W. Wu, D. Wei, J. Zhu, D. Niu, F. Wang, L. Wang, L. Yang, P. Yang, C. Wang, Enhanced electrochemical performances of organ-like Ti 3 C 2 MXenes/polypyrrole composites as supercapacitors electrode materials, Ceram. Int. 45 (2019) 7328–7337. doi:10.1016/j.ceramint.2019.01.016.

[19] Y. Xie, M. Naguib, V.N. Mochalin, M.W. Barsoum, Y. Gogotsi, X. Yu, K.W. Nam, X.Q. Yang, A.I. Kolesnikov, P.R.C. Kent, Role of surface structure on li-ion energy storage capacity of two-dimensional transition-metal carbides, J. Am. Chem. Soc. 136 (2014) 6385–6394. doi:10.1021/ja501520b.

[20] D. Rao, L. Zhang, Y. Wang, Z. Meng, X. Qian, J. Liu, X. Shen, G. Qiao, R. Lu, Mechanism on the Improved Performance of Lithium Sulfur Batteries with MXene-Based Additives, J. Phys. Chem. C. 121 (2017) 11047–11054. doi:10.1021/acs.jpcc.7b00492.

[21] X. Liu, X. Shao, F. Li, M. Zhao, Anchoring effects of S-terminated Ti2C MXene for lithium-sulfur batteries: A first-principles study, Appl. Surf. Sci. 455 (2018) 522–526. doi:10.1016/j.apsusc.2018.05.200.

[22] Y. Xie, Y. Dall'Agnese, M. Naguib, Y. Gogotsi, M.W. Barsoum, H.L. Zhuang, P.R.C. Kent, Prediction and characterization of mxene nanosheet anodes for non-lithium-ion batteries, ACS Nano. 8 (2014) 9606–9615. doi:10.1021/nn503921j.

[23] C. Du, J. Yeh, N. Pan, High power density supercapacitors using locally aligned carbon nanotube electrodes, 350 (2005). doi:10.1088/0957-4484/16/4/003.

[24] R.A. Mir, O.P. Pandey, Influence of graphitic/amorphous coated carbon on HER activity of low temperature synthesized B-Mo2C@C nanocomposites, Chem. Eng. J. 348 (2018) 1037–1048. doi:10.1016/j.cej.2018.05.041.

[25] G. Wang, L. Zhang, J. Zhang, A review of electrode materials for electrochemical supercapacitors, Chem. Soc. Rev. 41 (2012) 797–828. doi:10.1039/c1cs15060j.

[26] M. Ghidiu, M.R. Lukatskaya, M.Q. Zhao, Y. Gogotsi, M.W. Barsoum, Conductive two-dimensional titanium carbide "clay" with high volumetric capacitance, Nature. 516 (2015) 78–81. doi:10.1038/nature13970.

[27] M. Soleymaniha, M.A. Shahbazi, A.R. Rafieerad, A. Maleki, A. Amiri, Promoting Role of MXene Nanosheets in Biomedical Sciences: Therapeutic and Biosensing Innovations, Adv. Healthc. Mater. 8 (2019). doi:10.1002/adhm.201801137.

[28] B. Xiao, Y.C. Li, X.F. Yu, J.B. Cheng, MXenes: Reusable materials for NH 3 sensor or capturer by controlling the charge injection, Sensors Actuators, B Chem. (2016). doi:10.1016/j.snb.2016.05.062.

[29] J. Guo, Q. Peng, H. Fu, G. Zou, Q. Zhang, Heavy-Metal Adsorption Behavior of Two-Dimensional Alkalization-Intercalated MXene by First-Principles Calculations, J. Phys. Chem. C. 119 (2015) 20923–20930. doi:10.1021/acs.jpcc.5b05426.

[30] R. Paradiso, G. Loriga, N. Taccini, A Wearable Health Care System Based on Knitted Integrated Sensors, 9 (2005) 337–344.

[31] X. He, X. Hu, T.D. James, Chem Soc Rev Multiplexed photoluminescent sensors : towards improved disease diagnostics, (2017). doi:10.1039/c6cs00778c.

[32] C.E. Ren, M.Q. Zhao, T. Makaryan, J. Halim, M. Boota, S. Kota, B. Anasori, M.W. Barsoum, Y. Gogotsi, Porous Two-Dimensional Transition Metal Carbide (MXene) Flakes for High-Performance Li-Ion Storage, ChemElectroChem. 3 (2016) 689–693. doi:10.1002/celc.201600059.

[33] M. Pandey, K.S. Thygesen, Two-Dimensional MXenes as Catalysts for Electrochemical Two-dimensional MXenes as Catalysts for Electrochemical Hydrogen Evolution : A Computational Screening Study, (2017).

3.1. Raw Materials

In the present work, titanium (Alfa Aesar), aluminum (SD Fine Chemicals Pvt. Ltd) and graphite (Sigma Aldrich) are used as raw chemicals for the synthesis of Ti_3AlC_2 MAX phase. All chemicals were used without any further purification.

3.2. Methodology

The experimental details such as starting precursors, ball milling time, sintering and characterization are presented in flow chart to understand the process to synthesize the Ti_3AlC_2 MAX phase (Fig. 3.1).

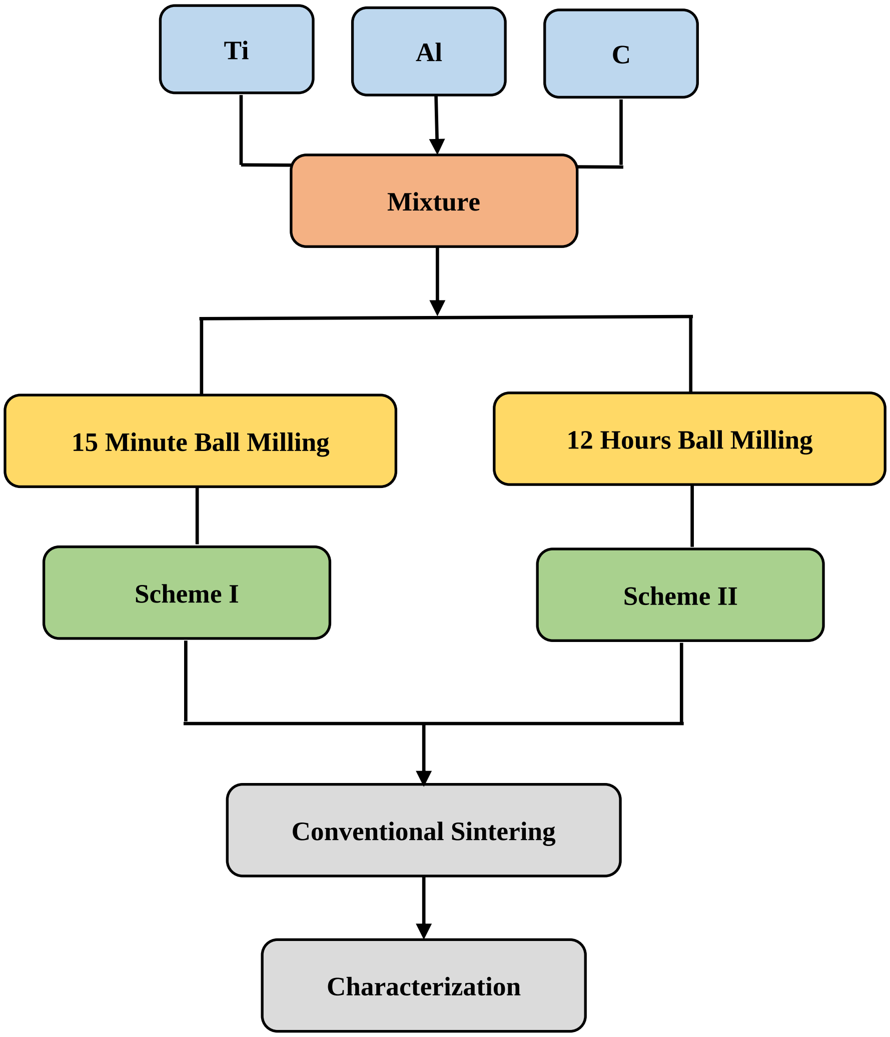

Fig. 3.1: Flow chart for the synthesis of Ti_3AlC_2 MAX phase.

According to the synthesis process, the experiments were performed by following two different experimental schemes based on the placement of the sample in the furnace. In scheme I, the powders were dry milled for 15 minutes at 350 rpm in a tungsten carbide jar (100 ml) using

RESTCH PM-100 (Germany) ball mill. The charge ratio was 10:1. After ball milling, the powder samples were cold pressed to make pellets of ~ 10 mm diameter and ~ 3 mm thickness in a hydraulic press (*CAP-15T*, *Pciss*, *India*) by applying 200 MPa pressure. The prepared pellets were sintered in a tubular furnace (*LTF 18/75/300, Lenton Thermal Design, United Kingdom)* at 5°C/min heating rate in the presence of high purity argon. The pelletized sample was placed on alumina plate without any cover.

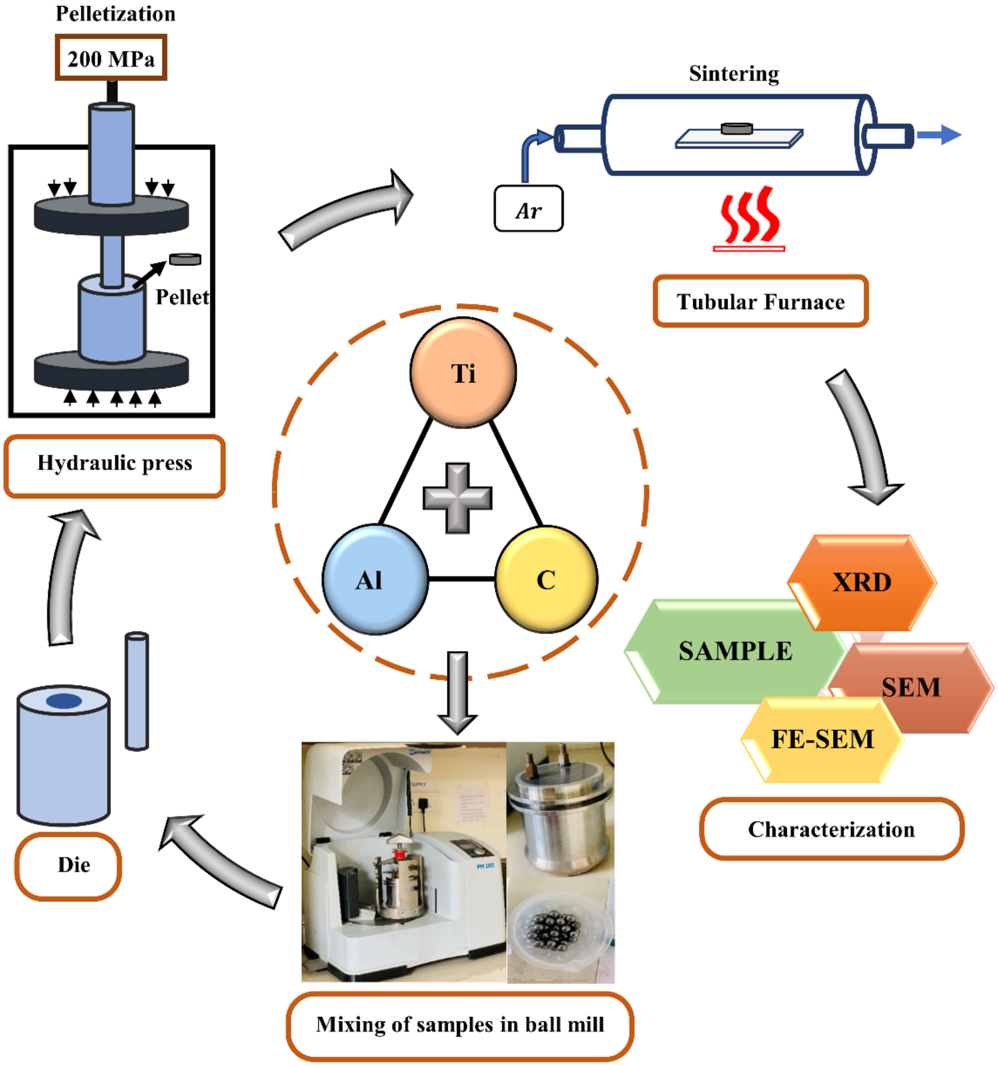

Fig. 3.2: Schematic representation for the synthesis of Ti_3AlC_2 MAX phase.

In scheme II, the powders were dry ball milled for 12 hours at 350 rpm under same conditions. The ball milling of the sample was performed in an argon atmosphere. The major difference in both the schemes was the placement of the pelletized sample in the tubular furnace. In this scheme, the pelletized sample was placed on alumina plate and covered with ball milled powder. Further, Fig. 3.2 shows the schematic representation for the synthesis of Ti_3AlC_2 MAX phase. The initial composition of different elements and sample naming in scheme I and scheme II are presented in Table 3.1. The samples were sintered at various temperatures by varying dwell time in both schemes to synthesize Ti_3AlC_2 MAX phase. The sintered samples of scheme I and scheme II were named, as presented in Table 3.2 – 3.3.

Table 3.1: The initial composition of elements and sample naming in scheme I and II.

SCHEME I			
Samples	**Precursors**		
	Ti	**Al**	**C**
TAC	3	1.3	1.9
SCHEME II			
TAC1	3	1.1	1.9
TAC2	3	1.4	1.9
TAC3	3	3	1.9
TAC4	5	5	1.9

Table 3.2: Sintered sample naming in scheme I.

Sample ID	**Temperatures (°C)**	**Dwell Time**
13 TAC	1300	1 hour
14 TAC	1400	
14.5 TAC	1450	

3.3. Material Characterization

3.3.1. X-ray Diffraction (XRD)

In the present work, the XRD diffraction analysis of prepared samples were studied by *PANalytical Xpert Pro* XRD diffractometer having Cu-Kα radiation source (λ= 1.5418 Å) operating at 45 kV/40 mA. The diffraction pattern of all synthesized samples placed in a sample holder were scanned in the defined 2θ range from 10° - 90° with step size of 0.0131. The corresponding peaks of all samples were identified by using *X'Pert Highscore* Plus software with reference to International Centre for Diffraction Data (ICDD) cards.

Table 3.3: Sintered sample naming in scheme II.

Sample ID	Temperatures (°C)	Dwell Time
8 TAC1-0.5	800	30 minutes
11 TAC1-0.5	1100	
13 TAC1-0.5	1300	
15 TAC1-0.5	1500	
8 TAC2-0.5	800	
11 TAC2-0.5	1100	
13 TAC2-0.5	1300	
15 TAC2-0.5	1500	
13.5 TAC3-1	1350	1 hour
14.5 TAC3-1	1450	
13 TAC4-1	1300	
14 TAC4-1	1400	
14 TAC4-0	1400	0 hour
13 TAC4-0	1300	
12.5 TAC4-0	1250	
12 TAC4-0	1200	
11 TAC4-0	1100	
10 TAC4-0	1000	

3.3.2. Scanning Electron Microscopy (SEM)

The surface morphology of the sample was studied by the SEM. In SEM, the electron beam is generated by an electron gun and collimated by electromagnetic lenses. The objective lenses are used to hit the surface of the sample for scanning and sample placed on the C-tape for analysis. The sample analysis was done with JEOL (JSM-IT100).

3.3.3. Field Emission Scanning Electron Microscopy (FE-SEM)

FE-SEM is generally used to study the surface morphology with high magnification. The sample preparation before the FE-SEM is important to get the good results. In the present work, pellet sample was placed on the C-tape for the analysis. The *HITACHI* –SU5000 apparatus was used to study the morphology of the sample with operating voltage of 15KV.

4.1. X-ray diffraction (XRD) analysis of scheme I

Figure 4.1 represents the formation of different phases in TAC sample ball milled for 15 minutes (Fig. 4.1a). The presence of titanium, aluminum and carbon phases is observed in TAC sample. This indicated that no reaction occurred between the starting precursor after ball milling. The sintering of the 13TAC, 14TAC and 14.5TAC samples was performed at 1300 °C (Fig. 4.1b), 1400 °C (Fig. 4.1c) and 1450 °C (Fig. 4.1d) for 1 hr dwell time in an argon atmosphere. XRD results demonstrated formation of distinct phases in 13TAC, 14TAC and 14.5TAC samples. At 1300 °C (Fig. 1b), formation of oxides (TiO and Al_2O_3) occurs along with minor phase of Ti_3Al. There was no signature associated with the formation of Ti_3AlC_2 MAX phase. The results revealed that oxidation occurred in 13TAC sample. Similar results were also obtained in 14TAC and 14.5TAC samples sintered at 1400 °C (Fig. 4.1c) and 1450 °C (Fig. 4.1d). The volume fraction of different phases (TiO, C, Al_2O_3, Ti_3Al, Ti, Al) are summarized in Table 4.1.

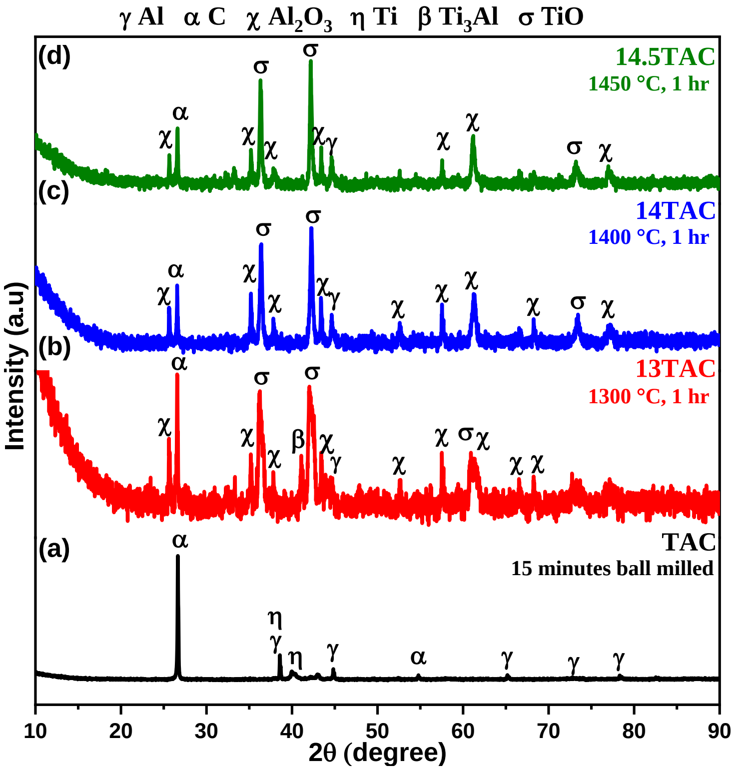

Fig. 4.1: XRD pattern of (a) TAC sample after ball milling and sintered samples (b) 13TAC, (c) 14TAC and (d) 14.5TAC.

According to Table 4.1, the volume fraction of TiO, C and Al_2O_3 increased with increase in sintering temperature from 1300 °C to 1450 °C. Also, the presence of Ti_3Al phase was observed only at 1300 °C. On the other hand, the volume fraction of Al decreased with increase in sintering temperature. It was clearly observed from Fig. 1 and Table 1 that the oxidation occurred in sintered samples due to which no peak associated with MAX phase was observed. Therefore, it was crucial to change the synthesis scheme to obtain Ti_3AlC_2 MAX phase.

Table 4.1: Volume fractions of phases present in TAC, 13TAC, 14TAC and 14.5TAC samples.

Sample ID	Volume Fraction (%)					
	Al_2O_3	Ti_3Al	TiO	Al	C	Ti
TAC	−	−	−	7.312	43.47	49.21
13TAC	31.72	3.123	50.56	6.559	6.774	−
14TAC	32.29	−	54.85	6.078	6.689	−
14.5TAC	33.88	−	55.60	3.842	6.668	−

According to Table 4.1, the volume fraction of TiO, C and Al_2O_3 increased with increase in sintering temperature from 1300 °C to 1450 °C. Also, the presence of Ti_3Al phase was observed only at 1300 °C. On the other hand, the volume fraction of Al decreased with increase in sintering temperature. It was clearly observed from Fig. 1 and Table 1 that the oxidation occurred in sintered samples due to which no peak associated with MAX phase was observed. Therefore, it was crucial to change the synthesis scheme to obtain Ti_3AlC_2 MAX phase.

4.2. X-ray diffraction (XRD) analysis of scheme II

In this scheme, the ball milling time was increased from 15 minutes to 12 hr. Fig 4.2 represents the presence of titanium (Ti), aluminium (Al) and carbon (C) phases in TAC1 and TAC2 samples after 12 hr ball milling. The Al content was varied from stoichiometry ratio in both the sample. In TAC1 (Fig. 4.2a) sample, 1.1 Al content was used from stoichiometry ratio, while 1.4 Al content was used in TAC2 (Fig. 4.2b) sample. The extra Al content was considered to overcome the loss during synthesis of MAX phase. The volume fraction of present phases was also calculated and presented in Table 4.2. It was observed that the fraction of Al content in XRD was more in TAC2 sample as compared to TAC1. The volume fraction of Ti decreased from 54.30 to 52.72 % with increased in Al content. However, the fraction of C remains the same in both the samples. According to scheme II, prepared pellets were covered with ball milled powders of corresponding sample during sintering. This helps to restrict the oxidation of sample, which will favour the formation of MAX phase. Moreover, sintering of TAC1 and TAC2 samples were performed at different temperature and time in an argon atmosphere. The XRD patterns of the samples (8TAC1, 8TAC2) sintered at 800 °C for 30 minutes dwell time are shown in Fig. 4.3.

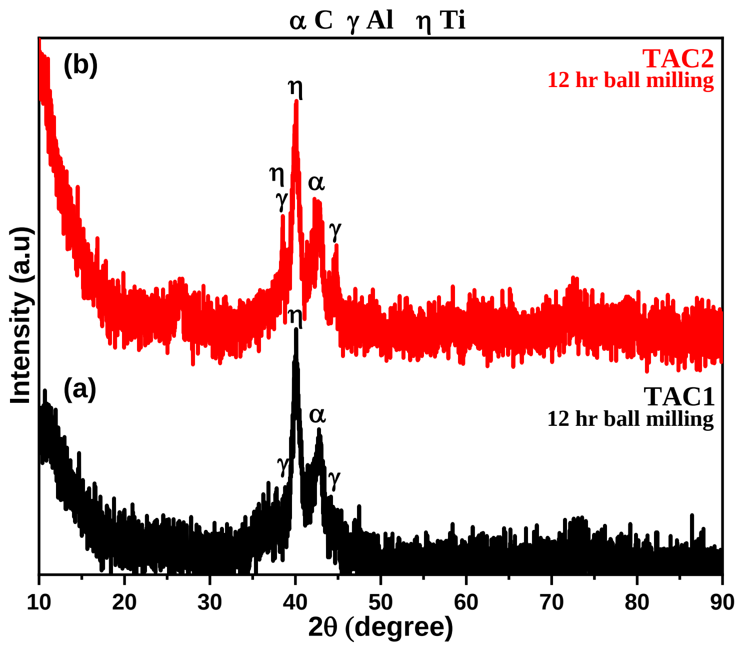

Fig. 4.2: XRD pattern of (a) TAC1and (b) TCA2 samples after 12 hr ball milling.

Table 4.2: Volume fraction of phases present in TAC1 and TAC2 samples.

Sample ID	Variation in Al (%)	Volume Fraction (%)		
		Al	C	Ti
TAC1	1.1	20.27	25.43	54.30
TAC2	1.4	22.49	25.74	52.72

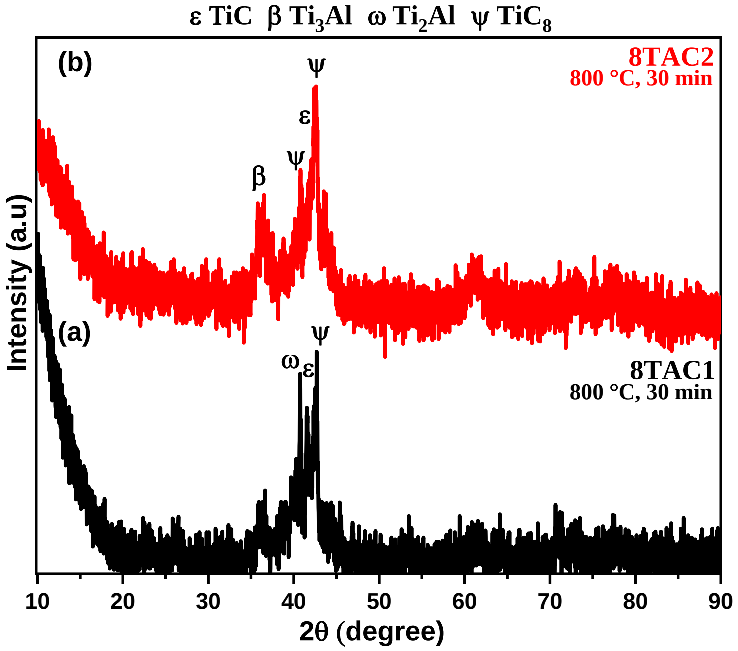

Fig. 4.3: XRD pattern of (a) 8TAC1and (b) 8TAC2 sintered samples.

The presence of TiC_8, TiC and Ti_2Al phases were observed in 8TAC1 sample (Fig. 4.3a). However, increased Al content in 8TAC2 sample (Fig. 4.3b) results into formation of Ti_3Al phase. The peak associated with TiC_8 and TiC phases were found to be more pronounced in 8TAC1 sample as compared to 8TAC2.

It was observed that the volume fraction of TiC_8 and TiC was decreased in 8TAC2 sample, as presented in Table 4.3. The formation of Ti_3AlC_2 phase was not observed in both the samples (8TAC1 and 8TAC2). The results indicated that the alloys of Ti-Al and Ti-C requires more energy to transform into Ti_3AlC_2 MAX phase. Therefore, TAC1 and TAC2 samples were sintered at higher temperatures (1100, 1300 and 1500 °C) for 30 minutes dwell time.

Table 4.3: Volume fraction of phases present in 8TAC1 and 8TAC2 sintered samples.

Sample ID	Al Content	Volume Fraction (%)				
		Ti_2Al	Ti_3Al	TiC_8	TiC	C
8TAC1	1.1	15.51	−	61.23	23.25	−
11TAC1		−	−	−	78.24	21.75
13TAC1		−	−	−	84.04	15.95
15TAC1		−	−	−	88.17	11.82
8TAC2	1.4	−	39.85	40.00	20.13	−
11TAC2		−	−	−	76.49	20.79
13TAC2		−	−	−	86.45	13.54
15TAC2		−	−	−	83.28	16.71

Figure 4.4 shows the XRD pattern of 11TAC1 (Fig. 4.4a), 13TAC1 (Fig. 4.4b) and 15TAC1 (Fig. 4.4c) sintered samples at 1100°C, 1300°C and 1500°C for 30 minutes holding time. The TiC phase was observed as a major phase in all the sintered samples (11TAC1, 13TAC1 and 15TAC1). A small peak related to C was also observed in Fig. 4.4. The volume fraction of TiC (Table 4.3) was found to be maximum in 15TAC1. However, the volume fraction of C decreased with increase in sintering temperature. This might be due to more diffusion of C into Ti at higher temperatures. It was also observed that at higher temperature Ti-Al alloys deforms due to evaporation of Al. So, excess Al content is required to compensate the Al during sintering. These results indicated that 1.1 Al content from stoichiometry is not enough for the synthesis of Ti_3AlC_2 MAX phase. Therefore, 1.4 Al (TAC2) content was considered to prepare MAX phase. Figure 4.5 shows the XRD diffractograms of 11TAC2 (Fig. 4.5a), 13TAC2 (Fig. 4.5b) and 15TAC2 (Fig. 4.5c) samples

sintered at 1100°C, 1300°C and 1500°C for 30 minutes. In these samples, 1.4 Al content was used. Similar results were obtained in the sintered samples with 1.1 and 1.4 Al content. This clearly indicated that Al content should be increased to obtain MAX phase.

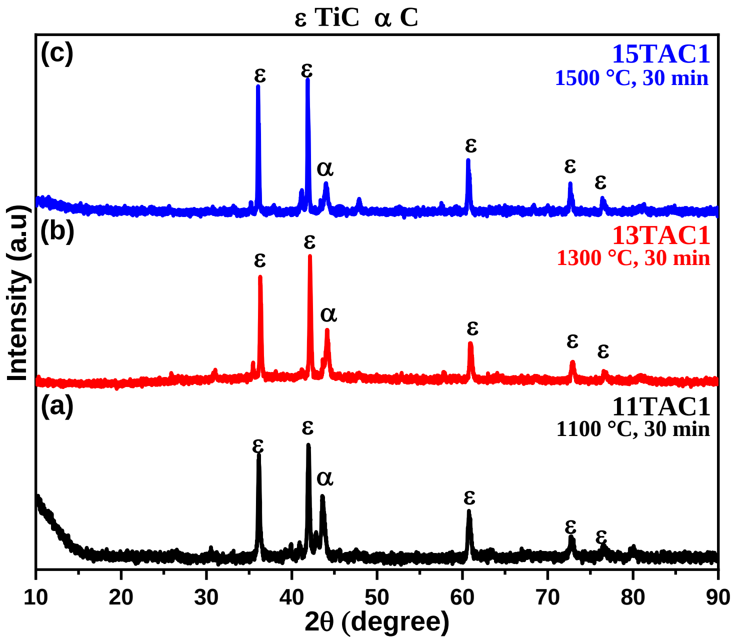

Fig. 4.4: XRD pattern of (a) 11TAC1, (b) 13TAC1 and (c) 15TAC1 sintered samples.

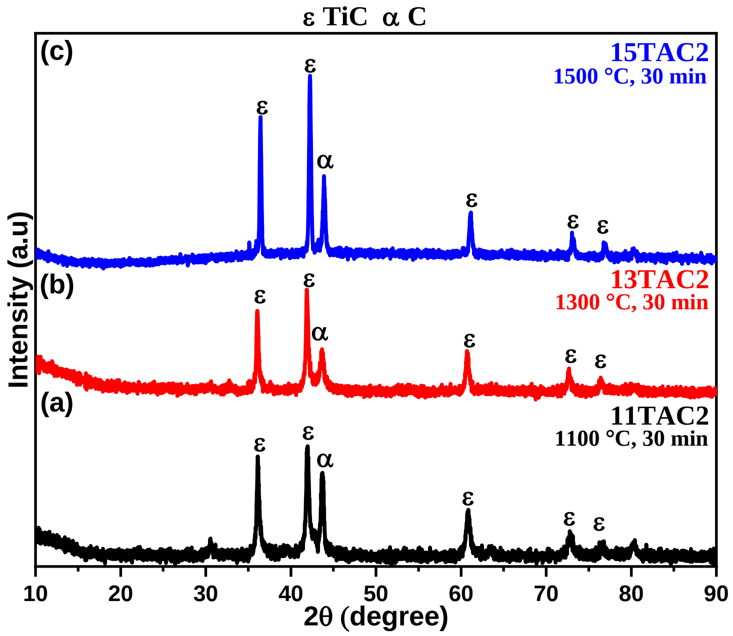

Fig. 4.5: XRD pattern of (a) 11TAC2, (b) 13TAC2 and (c) 15TAC2 sintered samples.

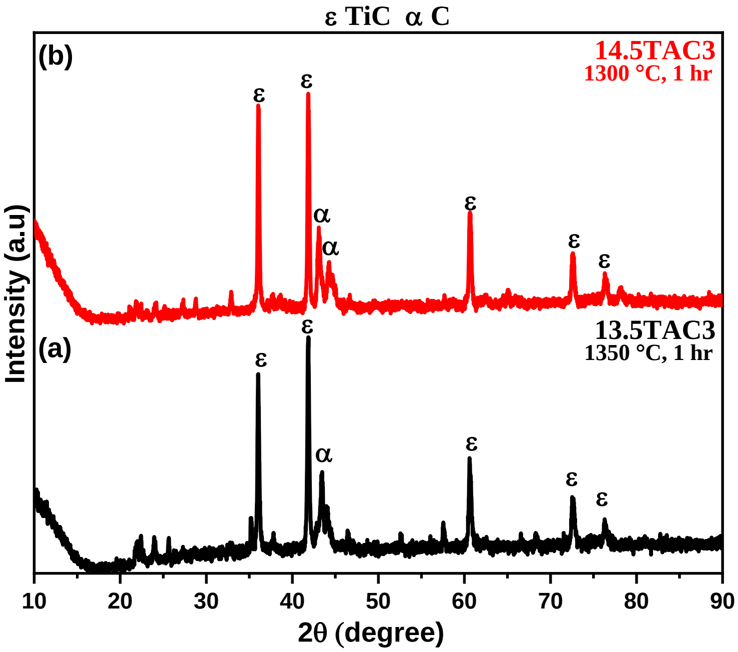

Fig. 4.6: XRD pattern of (a) 13.5TAC3 and (b) 14.5TAC3 sintered samples.

Afterwards, Al content was increased 3 times in TAC3 sample to prepare Ti_3AlC_2 MAX phase. Figure 4.6 shows the phase formation in 13.5TAC3 and 14.5TAC3 samples sintered at 1350°C and 1450°C for 1 hr. The results revealed the formation of titanium carbide (TiC) as a major phase and C as secondary phase. The volume fraction calculated for 13.5TAC3 and 14.5TAC3 samples is presented in Table 4.4. There was no peak observed related to MAX phase in the XRD patterns (Fig. 4.6). Therefore, Al content was further increased to 5 times of stoichiometry ratio in TAC4 sample.

Table 4.4: Volume fraction of phases present in 13.5TAC3 and 14.5TAC3 sintered samples.

Sample ID	Volume Fraction (%)	
	C	TiC
13.5TAC3	23.56	76.43
14.5TAC3	18.48	81.51

The TAC4 sample was sintered at 1300 °C and 1400 °C for 0 hr and 1 hr holding time. Fig. 4.7 shows the XRD pattern of 13TAC4-0 and 13TAC4-1 sintered samples at 1300°C for 0 and 1 hr holding. The results depicted the formation of Ti_3AlC_2 MAX phase as primary phase and four different phases (Ti_3AlC, Al_3Ti, Ti_3AlC_2 and C) as secondary phases after sintered at 1300°C. However, the volume fraction of Ti_3AlC_2 decreases from 31.84 to 26.59 % due to increases the holding time. The variation in volume fraction of other secondary phases are shown in Table 4.5.

Table 4.5: Volume fraction of phases present in 13TAC4-0, 13TAC4-1, 14TAC4-0, 14TAC4-1 and 12.5TAC4-0 sintered samples.

Sample ID	Volume Fraction (%)				
	Ti_3AlC_2	TiC	C	Al_3Ti	Ti_3AlC
13TAC4-0	31.84	55.32	5.751	1.240	5.829
13TAC4-1	26.59	62.97	3.973	1.094	5.370
14TAC4-0	23.20	46.61	3.661	2.162	24.35
14TAC4-1	19.54	58.35	8.226	1.788	12.29
12.5TAC4	48.12	42.00	5.264	2.197	2.467

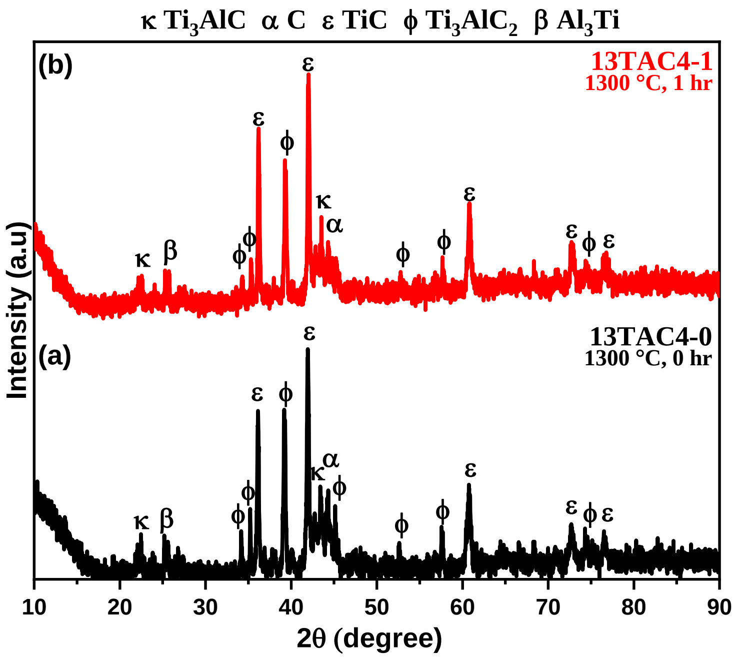

Fig. 4.7: XRD pattern of (a) 13TAC4-0 and (b) 13TAC4-1 sintered samples.

Figure 4.8 represents the XRD pattern of 14TAC4-0 and 14TAC4-1 sintered samples at 1400 °C for 0 hr and 1 hr. The results of XRD revealed the formation of phases TiC, Ti_3AlC, Al_3Ti, Ti_3AlC_2 and C. However, TiC is present as primary phase and other phases were present as secondary phase. The volume fraction of the Ti_3AlC_2 MAX phase and Ti_3AlC decreases with increase in holding time. It is observed that 0 hr holding time favors the formation of Ti_3AlC_2 MAX phase. More intense peaks related to Ti_3AlC_2 MAX phase were observed in 13TAC4-0 sample. This clearly indicated that lower temperature favors the formation of Ti_3AlC_2 MAX phase.

The volume fraction of the Ti_3AlC_2 MAX phase and Ti_3AlC decreases with increase in holding time. It is observed that 0 hr holding time favors the formation of Ti_3AlC_2 MAX phase.

More intense peaks related to Ti_3AlC_2 MAX phase were observed in 13TAC4-0 sample. This clearly indicated that lower temperature favors the formation of Ti_3AlC_2 MAX phase. Also, the content of Al in TAC4 seems to be enough for the synthesis of Ti_3AlC_2 MAX phase. Furthermore, TAC4 sample was sintered at lower temperatures 1250, 1200 and 1100 °C for 0 hr dwell time.

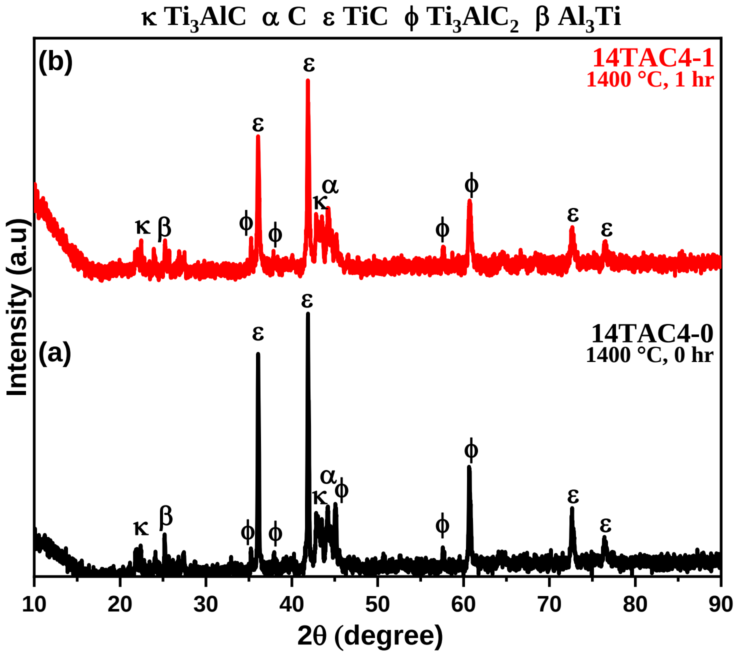

Fig. 4.8: XRD pattern of (a) 14TAC4-0 and (b) 14TAC4-1 sintered samples.

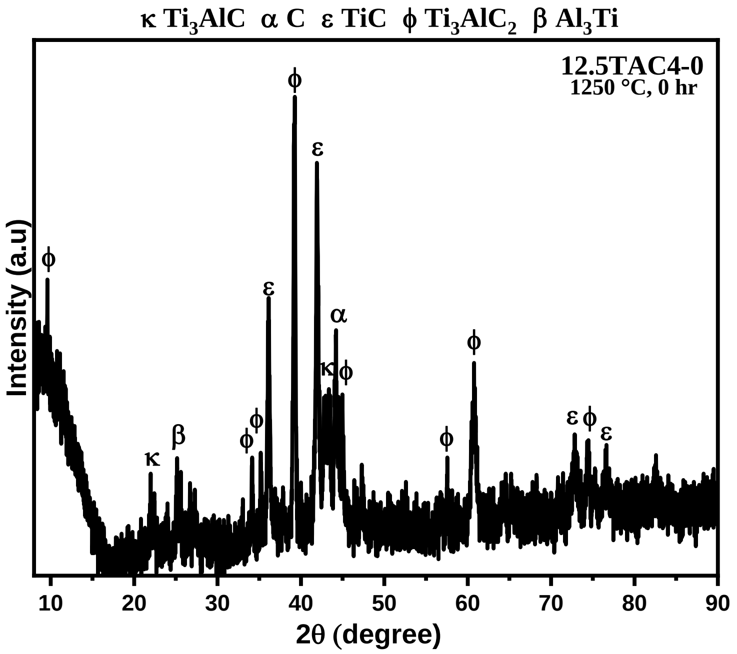

Fig. 4.9: XRD pattern of 12.5TAC4-0 sintered sample.

Figure 4.9 represents the XRD pattern of 12.5TAC4-0 sample sintered at 1250°C for 0 hr. The results of XRD revealed the formation of Ti_3AlC_2 MAX phase as primary phase. However, TiC, Ti_3AlC, Al_3Ti, Ti_3AlC_2 and C still present as secondary phases. Best results were obtained in 12.5TAC4-0 sample sintered at 1250 °C for 0 hr. Also, the volume fraction (Table 4.5) of Ti_3AlC_2 MAX was maximum in the case of 12.5TAC4-0 sample.

4.3. Fractured surface morphology of sintered samples

The fractured surface morphology of the best synthesized samples (11TAC4-0, 12TAC4-0, and 12.5TAC4-0) was investigated through SEM and FE-SEM. Fig 4.10 shows the SEM micrographs of samples 11TAC4-0 (Fig. 4.10a-b), 12TAC4-0 (Fig. 4.10c-d) and 12.5TAC4-0 (Fig. 4.10e-f) sintered at 1100 °C, 1200 °C and 1250 °C for 0 hr dwell time.

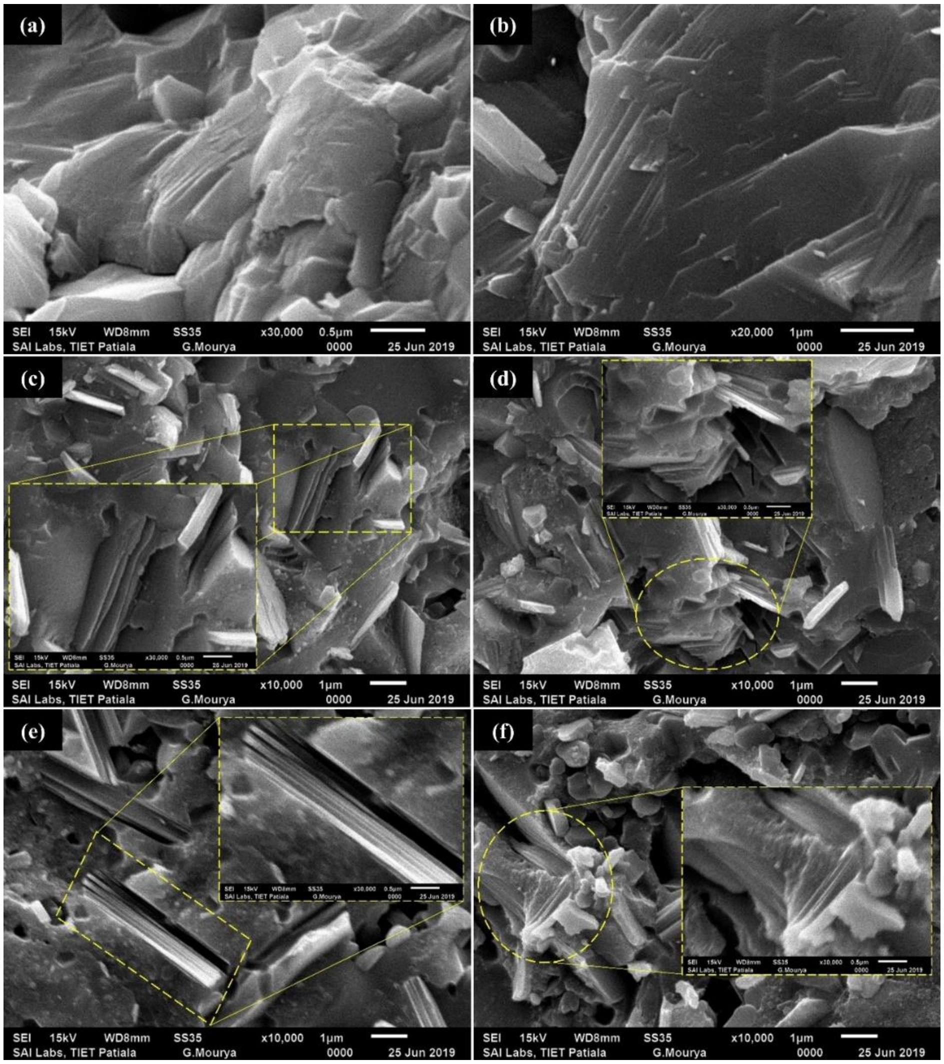

Fig. 4.10: SEM micrographs of (a-b) 11TAC4-0, (c-d) 12TAC4-0 and (e-f) 12.5TAC4-0 sintered samples.

It was observed from Fig. 4.10 that the nanolaminated structure appears in all three samples. The nanolaminated structure is a typical signature of MAX phases [1-4]. This also confirms the formation of Ti_3AlC_2 MAX phase. However, increase in sintering temperature results into breaking of layers. Fig. 4.10e-f represents breaking of layers at higher temperature (1250 °C). The best results were obtained in 12TAC4-0 sample (Fig. 4.10c-d) as compared to 11TAC4-0, and 12.5TAC4-0 samples.

To gain more information on the fractured surface of prepared sample, FE-SEM analysis was performed. Fig 4.11 shows the FE-SEM micrographs of 12TAC4-0 (Fig. 4.11a-b) and 12.5TAC-0 (Fig. 4.11c-d) sintered samples. The FE-SEM results show nanolaminated structure in 12 TAC4-0 sample. At 1250 °C, layered structure breaks. FE-SEM results are in agreement with SEM results.

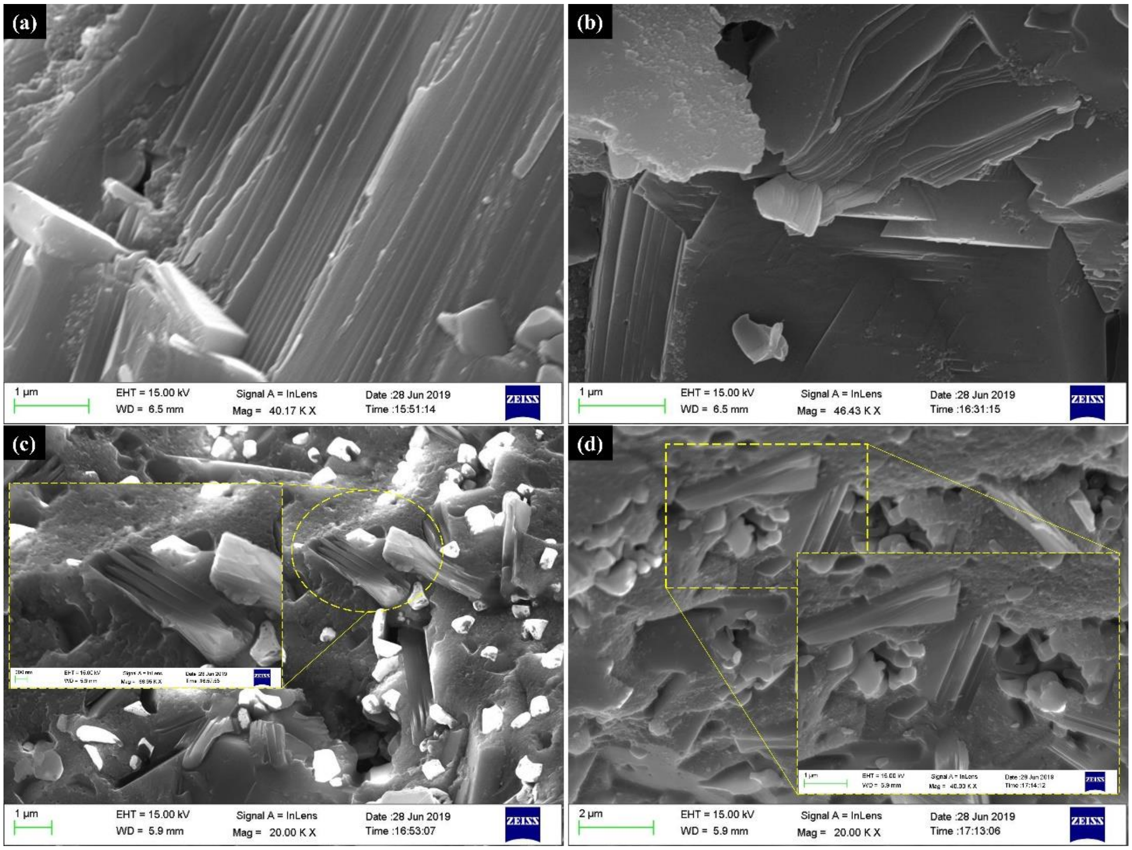

Fig. 4.11: FE-SEM micrographs of 12TAC4-0 (Fig. 4.11a-b) and 12.5TAC-0 (Fig. 4.11c-d) sintered samples.

References

[1] W. Wu, D. Wei, J. Zhu, D. Niu, F. Wang, L. Wang, L. Yang, P. Yang, C. Wang, Enhanced electrochemical performances of organ-like Ti_3C_2 MXenes/polypyrrole composites as supercapacitors electrode materials, Ceram. Int. 45 (2019) 7328–7337. doi:10.1016/j.ceramint.2019.01.016.

[2] G. Gao, A.P. O'Mullane, A. Du, 2D MXenes: A New Family of Promising Catalysts for the Hydrogen Evolution Reaction, ACS Catal. 7 (2017) 494–500. doi:10.1021/acscatal.6b02754.

[3] R. Liu, W. Cao, D. Han, Y. Mo, H. Zeng, H. Yang, W. Li, Nitrogen-doped Nb_2CT_x MXene as anode materials for lithium ion batteries, J. Alloys Compd. 793 (2019) 505–511. doi:10.1016/j.jallcom.2019.03.209.

[4] R. Cheng, T. Hu, H. Zhang, C. Wang, M. Hu, J. Yang, C. Cui, T. Guang, C. Li, C. Shi, P. Hou, X. Wang, Understanding the Lithium Storage Mechanism of $Ti_3C_2T_x$ MXene, J. Phys. Chem. C. 123 (2019) 1099–1109. doi:10.1021/acs.jpcc.8b10790.

5.1. Conclusions

The Ti_3AlC_2 MAX phase was successfully synthesized along with TiC impurity through conventional sintering technique. In scheme I, titanium, aluminum and carbon were ball milled for 15 minutes and sintered at 1300°C, 1400°C and 1450°C. The XRD pattern revealed that the formation of TiO occurred in all sintered samples. This indicated that the oxidation of the samples occurred during sintering. Therefore, the synthesis scheme was changed to prepare Ti_3AlC_2 MAX phase. In scheme II, same precursors were ball milled for 12 hours and the pelletized samples were covered with ball milled powders before sintering at various temperatures. This resulted into increase in resistance towards oxidation and formation of non-oxide phases was observed. In addition, effect of change in composition on the synthesis of Ti_3AlC_2 MAX phase was studied. The Ti_3AlC_2 MAX phase was obtained after sintering of TAC4 (Ti/Al/C = 5/5/1.9) sample. The surface morphology of the samples was confirmed through SEM and FE-SEM. The best results were obtained the 12TAC4-0 sample sintered at 1200 °C for 0 hr holding time. The study provides substantial route to prepare MAX phases.

5.2. Future Scope

The synthesis parameters (Ball mill duration, sintering temperature, dwell time, and composition) should be optimized to obtain nanolaminated Ti_3AlC_2 MAX phase. Also, the Ti_3C_2 MXene could be obtain through etching of pure Ti_3AlC_2. The impact of different etching agent on the morphology and properties of MXenes could be investigated. Further, to enhance the capacitance of MXenes intercalation and delamination could be done with different organic molecules. In the end, electrochemical properties of MXenes should be explored.